Available online at www.sciencedirect.com
SCIENCE DIRECT®
C. R. Physique 4 (2003) 1009–1019
COMPTES RENDUS PHYSIQUE

Carbon nanotubes: state of the art and applications/Les nanotubes de carbone : état de l'art et applications

Electronic structure of carbon nanotubes

Philippe Lambin

Département de physique, facultés universitaires N.D. de la paix, 61, rue de Bruxelles, B 5000 Namur, Belgium

Presented by Guy Laval

Abstract

This paper is a review of the theoretical and experimental studies devoted so far to the electronic structure of pure carbon nanotubes, including single-wall, multiwall, and ropes of single-wall nanotubes. A universal picture of the band structure of single-wall nanotubes is obtained by exploiting a particular helical symmetry. A brief description of the optical properties of the nanotubes is also presented. Potential applications of carbon nanotubes in nanoelectronics are described. ***To cite this article: Ph. Lambin, C. R. Physique 4 (2003).***

Résumé

Structure électronique des nanotubes de carbone. Cet article est une revue des acquis théoriques et expérimentaux sur la structure électronique des nanotubes de carbone, à la fois pour les tubes monofeuilles, multifeuillets et les faisceaux de nanotubes. Une vue unifiée de la structure de bandes électroniques des nanotubes monofeuillets est obtenue par application d'une symétrie hélicoïdale particulière. Une brêve description des propriétés optiques des nanotubes est aussi présentée. Les applications possibles des nanotubes de carbone en nanoélectronique sont décrites. ***Pour citer cet article : Ph. Lambin, C. R. Physique 4 (2003).***

Keywords: Carbon nanotubes; Electron band structure; Joint density; Nanoelectronics

Mots-clés : Nanotubes de carbone ; Structure de bandes électroniques ; Nanoélectronique

1. Introduction

One of the most spectacular properties of single-wall carbon nanotubes is that they can be metallic or semi-conducting depending on their helicity [1–4]. Possible applications of nanotubes in nano-electronic devices will exploit that property [5]. On a more fundamental point of view, the fact that the nanotubes are one-dimensional systems brings interesting phenomena. More exactly, carbon nanotubes are quasi one-dimensional systems: the atoms are located on a cylindrical surface in three-dimensional space; they do not form a one-dimensional chain, like for instance in polyacetylene. This remark is important because the Peierls instability that is responsible for alternating simple and double bonds in polyacetylene for example, and to open a gap of 1.4 eV there [6], is inoperant in the case of carbon nanotubes [1,7,8]. Other one-dimensional effects are predicted to occur in metallic nanotubes, such as the breakdown of the usual Fermi liquid description in favour of Tomonaga–Luttinger behavior dominated by collective excitations [9].

This paper is a review of the usual, one-electron properties of pure carbon nanotubes. After a rapid survey of the elementary graphene zone folding theory (Section 2), a unified picture of the electron band structure of single-wall nanotubes (SWNT) is presented in Section 3. The consequences of the band structure on optical properties of SWNTs are briefly outlined in

E-mail address: philippe.lambin@fundp.ac.be (Ph. Lambin).

1631-0705/$ – see front matter
doi:10.1016/S1631-0705(03)00101-4

Section 4. The electronic properties of ropes of single-wall nanotubes and of multiwall nanotubes are reviewed in Section 5. A short description of possible applications of SWNTs in nanoelectronics is the subject of Section 6.

2. Zone folding of the π bands of graphene

Conceptually, a single-wall nanotube is a rolled-up stripe of graphene from which it retains part of its electronic structure. Close to the Fermi energy, the band structure of graphene is dominated by the π states formed by the interacting $2p_z$ orbitals normal to the graphene sheet [10]. Since there are two atoms in the unit cell of graphene, there are two π bands, a bonding (π) one and an anti-bonding (π^*) one. These bands cross each other at the corners of the hexagonal first-Brillouin zone, the K points. For symmetry reasons, the Fermi level coincides with the energy of the crossing. Graphene is a zero-gap semiconductor; its density of states (DOS) at the Fermi energy E_F is zero and increases linearly on both sides of E_F. A contour plot of the π band in the reciprocal plane of graphene is shown in Fig. 1.

In a nanotube, cyclic boundary conditions apply around the circumference. In the planar development of the (n, m) nanotube, the circumference is the wrapping vector $\vec{C}_h = n\vec{a}_1 + m\vec{a}_2$, where $\vec{a}_1$ and $\vec{a}_2$ are two primitive translation vectors of graphene, which by convention make an angle of 60° between them. In the two-dimensional graphene sheet, the wave function at the end point of $\vec{C}_h$ is the one at the origin multiplied by the Bloch factor $\exp(\mathrm{i}\vec{k}\cdot\vec{C}_h)$. Assuming that the graphene wavefunctions remain valid in the rolled up structure, the cyclic boundary conditions impose $\exp(\mathrm{i}\vec{k}\cdot\vec{C}_h) = 1$. That condition discretizes the Bloch vector $\vec{k}$ along equidistant lines $\vec{C}_h \cdot \vec{k} = \ell 2\pi$ perpendicular to $\vec{C}_h$, and therefore parallel to the nanotube axis, where ℓ is an integer number. These discretization lines are drawn in Fig. 1. Along each of these lines, the π and π^* bands of graphene are probed. These two bands are always separated by a gap unless one of the discretization line passes through a corner K of the first-Brillouin zone. The nanotube is then a metal because it contains two bands that cross the Fermi level. This happens when $nK_1 + mK_2 = \ell$, where K_1 and K_2 are the coordinates of a K point in the basis of the reciprocal unit vectors of graphene. Taking for instance $K_1 = 1/3$ and $K_2 = -1/3$ leads to the condition that $n - m$ must be a multiple of 3 to obtain a metallic nanotube [2]. Otherwise it is a semiconductor.

The band gap E_g of semiconductor nanotube is easy to estimate when it is assumed that the dispersion of the π and π^* bands is isotropic and linear around a K point:

$$E = \pm\hbar v_F \delta k \tag{1}$$

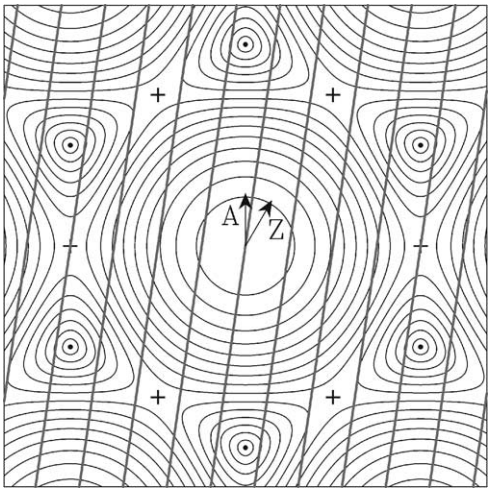

Fig. 1. Contour plot of the bonding π band in the reciprocal plane of graphene. The Γ point is at the center of the figure, the corners K of the first Brillouin zone are indicated by the black dots, the M points are indicated by the crosses. The thick lines across the drawing are discretization lines of the the Bloch vector for the (5,3) nanotube. The two arrows indicate the axial direction of the armchair (A) and zig–zag (Z) nanotubes.

Fig. 1. Lignes de contour de la bande π liante dans l'espace réciproque du graphène. Le point Γ est au centre de la figure, les sommets K de la première zone de Brillouin sont indiqués par des ronds noirs et les points M par des croix. Les lignes grasses qui traversent la figure sont les lignes de discrétisation du vecteur de Bloch pour le nanotube (5,3). Les deux flèches indiquent la direction axiale des tubes 'armchair' (A) et zig–zag (Z).

Table 1
Electronic properties of the single-wall nanotube (n, m). In the formulas d and θ are the diameter and chiral angle, $d_{CC} = 0.142$ nm is the nearest-neighbor distance in graphite, E_g is the band gap of the semiconducting tubes, $c_g \approx 3.1$ eV [18], $n(E_F)$ is the density of states per atom at the Fermi level for the metallic tubes, and $\gamma_0 = 2.9$ eV is the π-electron interaction. The last line gives the positions of the van Hove singularities close to the Fermi level ($\ell = 1, 2, 3, \ldots$), which are symmetrically located on both sides of E_F.

$n - m \neq \mathcal{M}(3)$	$n - m = \mathcal{M}(3) \neq 0$	$n - m = 0$
semiconductor	small-gap semiconductor	metal
$E_g = 2\gamma_0 d_{CC}/d$	$E_g = c_g \lvert\cos(3\theta)\rvert (d_{CC}/d)^2$	$n(E_F) = 2\sqrt{3} d_{CC}/(\pi^2 \gamma_0 d)$
$\lvert E_{2\ell-1}\rvert = (3\ell - 2)\gamma_0 d_{CC}/d$	$\lvert E_\ell\rvert = 3\ell\gamma_0 d_{CC}/d$	$\lvert E_\ell\rvert = 3\ell\gamma_0 d_{CC}/d$
$\lvert E_{2\ell}\rvert = (3\ell - 1)\gamma_0 d_{CC}/d$		

with v_F the Fermi velocity. In the above formula, δk is the distance of the Bloch vector to the K point and E is the energy with respect to the Fermi level. As can be seen in Fig. 1, the closest distance of the discretization lines to a K point is one third the separation between these lines, which is the reciprocal of the nanotube radius $1/R$. By setting $\delta k = 1/3R$ in the above equation, one obtains $E_g = 2\hbar v_F/3R$. In the π orbital tight-binding approximation [10],

$$\hbar v_F = 3\gamma_0 d_{CC}/2, \tag{2}$$

where γ_0 is the absolute value of the $pp\pi$ hopping interaction (2.9 eV [11]) and d_{CC} is the CC distance (0.142 nm). This expression leads to the band gap given in Table 1. It is inversely proportional to the nanotube diameter [12].

In a metallic nanotube, the π and π^* bands that cross at the K point contribute $1/\pi|\mathrm{d}E/\mathrm{d}k|$ each to the density of states. Due to the linear dispersion of these bands, the density of states is a constant around the Fermi level (see Table 1). The bands coming from the next discretization lines that pass at a distance $1/R$ from the K point have their energy at least $\hbar v_F/R$ away from the Fermi level. This means that the metallic nanotubes have a plateau of constant density of states around E_F in an interval of width $2\hbar v_F/R$, three times as large as the band gap of a semiconductor with same radius. All these predictions about the density of states of the nanotube have been confirmed experimentally by scanning tunneling spectroscopy (STS) [13,14]. The linear dispersion of the π and π^* bands near E_F in the armchair nanotubes has also been demonstrated experimentally by the same technique [15,16].

The density of states of a nanotube is characterized by a series of van Hove singularities that occur at energies such that $\mathrm{d}E/\mathrm{d}k = 0$, where E is the energy of a band. Around the Fermi level, where the linear dispersion of Eq. (1) is valid, minima or maxima of the two bands sampled along a discretization line take place at the closest distance to the K point. For a semiconductor, the closest distance is $(\ell + 1/3)/R$ or $(\ell + 2/3)/R$, whereas for a metal, it is ℓ/R, with ℓ an integer. The positions of the van Hove singularities deduced from these relations are given in Table 1.

The above analysis based on the zone folding of graphene is essentially correct except that it neglect two effects. First, the linear and isotropic dispersion of the π and π^* bands is only true in a close neighborhood of the K points. At some distance from a K point, the energy contour lines are no longer circles but exhibit a trigonal anisotropy, see Fig. 1. This means that the formula of Table 1 are only valid for large diameters. Second, the effects of curvature were neglected. In a cylindrical geometry, the π orbitals are locally oriented along the normal to the nanotube and are not parallel to each other like in graphene. They mix with the σ orbitals of neighboring sites. This mixing, although small [7], lifts the degeneracy of the π and π^* states at the K point and a small gap opens in these nanotubes for which $n - m = M(3)$ [17–19], except for the armchair nanotubes (n, n) where the crossing of the bands at E_F is still allowed due to the C_{nv} symmetry for all Bloch wave vectors [8,20]. Effects of this small gap have been detected by far-infrared spectroscopy [21] and transport measurements [22]. The small gap, which is maximum in the zig–zag nanotubes (see Table 1), has been measured experimentally by STS [23].

3. Band structure of single-wall nanotubes

Soon after the discovery of the carbon nanotubes, band structure calculations of SWNTs have been performed with local-density functional theory using either localized orbitals [1] or plane-wave expansions [24,25]. Comparisons were made with simplest tight-binding calculations. The latter were shown to be unable to reproduce strong effects of σ–π hybridization in nanotubes with diameter below 0.6 nm [25], which shift down the π^* bands [26]. For nanotubes with diameters around 1.2 nm and above, the tight-binding band structure and density of states were shown to be fairly correct up to $\sim$1.5 eV above the Fermi level [20,26–29].

The tight-binding theory has the advantage that it is simple and the results it leads to are easily interpreted. In the Slater–Koster formalism, the tight-binding Hamiltonian requires a few parameters that can be fitted to ab-initio calculations or ad-

justed to experimental data. All the tight-binding calculations illustrated in this section were performed with the parameters of Mintmire and White [20]. This model incorporates the four valence orbitals of C in an orthogonal basis with first-neighbor interactions.

Carbon nanotubes are periodic systems along their axis. Except for the zig–zag and armchair geometry, the translation period can be large, with the consequence that the number of atoms per unit cell is large. The nanotubes possess screw operations which considerably reduce the number of atoms to use in band structure calculations [12].

In Fig. 2, the chain of atoms marked by the thick lines becomes a helix in the rolled up structure. This particular chain makes an angle $\pi/6+\theta$ with respect to the axial direction, where θ is the chiral angle of the nanotube. With the helical scheme adopted here, the complete nanotube can be generated from n ($m \geqslant 0$) or $n-|m|$ ($m<0$) such diatomic helices (when m is negative, the chain running along the dashed line marked with the ϕ angle must be used, see Fig. 2) [30]. To move from one atom represented by a circle in Fig. 2 to the next one along the same helix, it suffices to operate a primitive translation

$$\vec{h} = \vec{a}_2 \ (m \geqslant 0) \quad \text{or} \quad \vec{h} = \vec{a}_2 - \vec{a}_1 \ (m < 0). \tag{3}$$

On the rolled-up cylinder, this operation corresponds to a translation $\tau = 3n' d_{\mathrm{CC}}/2c$ along the axis, followed by a rotation $\alpha = \pm\pi(n'+2m')/c^2$ about the axis, where the $+$ sign corresponds to $m \geqslant 0$ and the $-$ sign to $m<0$. In these expressions $c = \sqrt{n^2+m^2+nm}$, $n'=n$ and $m'=m$ when $m \geqslant 0$, $n'=n+m$ and $m'=-m$ when $m<0$.

It is possible to use the screw operation $\hat{s}$ defined by τ and α in a generalized Bloch theorem, which states that $\hat{s}\psi = \exp(\mathrm{i}\kappa\tau)\psi$, with ψ a wave function of the nanotube, and $-\pi/\tau \leqslant \kappa \leqslant +\pi/\tau$ [20]. If again curvature effects are ignored, ψ is a Bloch function of graphene with some wavevector $\vec{k}$, the screw operation on the cylinder corresponds to the primitive translation $\vec{h}$ (Eq. (3)) of graphene and $\hat{s}\psi = \exp(\mathrm{i}\vec{k}\cdot\vec{h})\psi$ in the planar development. As a result,

$$\kappa\tau = \vec{k}\cdot\vec{h}. \tag{4}$$

When the screw operation is applied to connect an atom j to the atom i in the unit cell, the rotation α must be operated on the orbitals of atom j. With the screw operation defined here above, the unit cell contains $2n'$ atoms (two per helix). As mentioned above, other choices of helical symmetry are possible, which can reduce the number of atoms to as little as two [12,31]. The advantage here is that τ is always of the order of the C–C distance d_{CC}, which makes easy the comparison of the band structures of nanotubes with various chiralities. In fact, one is led to a unified description of the nanotube band structure, as we now show.

Fig. 3 shows the tight-binding band structure of a few nanotubes with different chiralities. For the (10,10) armchair nanotube, the electronic bands are represented in the first-Brillouin zone. For all the others, the screw operation introduced here above was applied to represent the band structure in an extended zone. For the metallic nanotubes, displayed on the right-hand side of the figure, the crossing of the π and π^* bands is taking place close to the $2/3$ of the ΓX zone. Except for the $(10,10)$ tube, the band crossing is avoided due to the curvature effects described in Section 2, but the splitting of the bands is hardly seen in the figure. The semiconducting nanotubes all have a direct gap, also located close to the $2/3$ of the ΓX zone. The reason for this is a consequence of Eqs. (3) and (4), given that at the corner K of the graphene first Brillouin zone, one has $\vec{k}_K \cdot \vec{h} = \pm 2\pi/3$. As

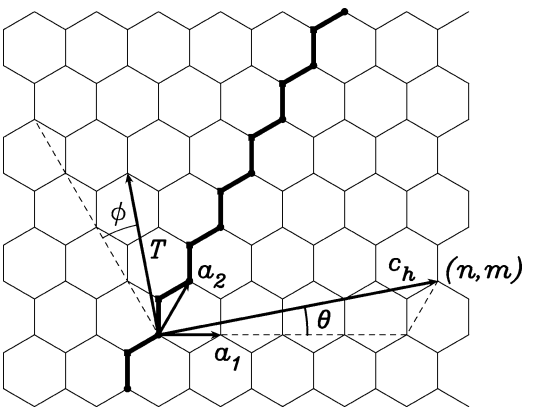

Fig. 2. Two-dimensional graphene sheet showing the circumference C_h and the true period T of the (n,m) nanotube, together with the chiral angle θ. The zig–zag chain of atoms highlighted by thick lines becomes an helix in the rolled up structure. It is composed of two atoms marked with circles and squares. n such helices completely define the atomic structure of the nanotube when $m \geqslant 0$.

Fig. 2. Feuile bi-dimensionnelle de graphène montrant la circonférence C_h et la période vraie T du nanotube (n,m), ainsi que l'angle chiral θ. La chaîne zig–zag d'atomes mise en évidence par les lignes grasses devient une hélice sur le tube. Elle est composée de deux atomes indiqués par des cercles et des carrés. n hélices de ce type définissent complètement la structure atomique du nanotube lorsque $m \geqslant 0$.

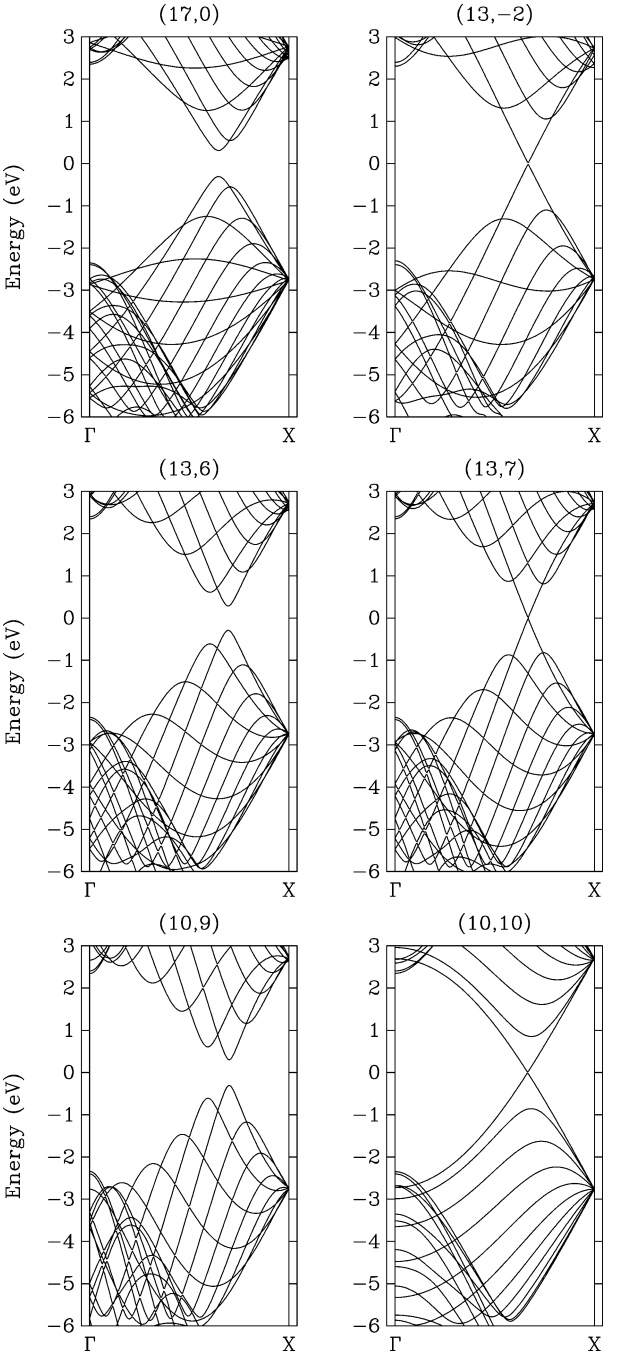

Fig. 3. Tight-binding band structure of six single-wall carbon nanotubes. The Bravais primitive cell was used for the $(10, 10)$ nanotube. For the other tubes, the screw operation described in the text was applied to represent the band structure in an extended Brillouin zone. The nanotubes on the left-hand side are semiconducting, the ones on the right-hand side are metallic, except for the small gap induced by curvature in $(13, -2)$ and $(13, 7)$. This band gap is 0.037 eV in the case of the small nanotube $(13, -2)$ ($d = 0.95$ nm). The Fermi level is at zero energy.

Fig. 3. Structure de bandes en liaisons fortes de six nanotubes monofeuillets. La cellule primitive de Bravais a été utilisée pour le nanotube $(10, 10)$. Pour les autres tubes, l'opération vis décrite dans le texte a été appliquée pour représenter la structure de bandes dans une zone étendue. Les nanotubes situés à gauche de la figure sont des semi-conducteurs, ceux à droite sont des métaux si l'on fait abstraction de la petite bande interdite ouverte par la courbure dans les tubes $(13, -2)$ et $(13, 7)$. Cette bande interdite est de 0.037 eV dans le cas du petit nanotube $(13, -2)$ ($d = 0.95$ nm). Le niveau de Fermi est au zéro d'énergie.

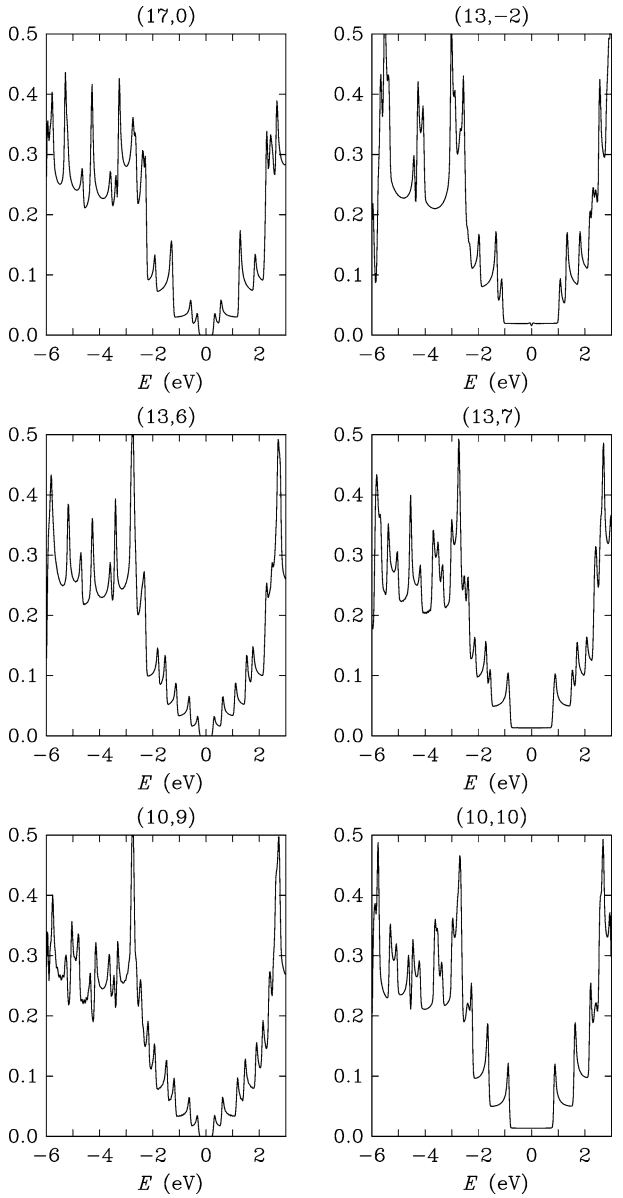

Fig. 4. Tight-binding density of states of the six nanotubes considered in Fig. 3. The Fermi energy is at 0.

Fig. 4. Densités d'états en liaisons fortes des six nanotubes considérés à la Fig. 3. Le niveau de Fermi est en 0.

it is also clear in Fig. 3, the π and π^* bands converge to nearly the same energy at the X point, $\sim \pm 2.8$ eV, which corresponds to the $pp\pi$ interaction. In graphene, the π and π^* bands have that energy at the M point. According to Eqs. (3) and (4), the M point corresponds to the X zone boundary of the nanotube, since $\vec{k}_M \cdot \vec{h} = \pm\pi$.

The densities of states of the same nanotubes as in Fig. 3 are shown in Fig. 4. The density of states is characterized by a series of van Hove singularities that are real fingerprints of the nanotube. Indeed, the precise location of these peaks can be used to identify a nanotube from its STS spectrum [32]. Near the Fermi level, their positions follow approximately the expressions given in Table 1 [27,33]. Except for the armchair geometry, there is a splitting of the van Hove peaks on both sides of the DOS plateau of the metallic nanotubes, which is due to the trigonal symmetry of the π and π^* bands around the K point [34]. The magnitude of the splitting is maximum for the zig–zag configuration. All the nanotubes present a DOS peak at about ± 2.8 eV. These peaks are the consequence of the accumulation of bands at the X point. They are reminiscent of the peak that the DOS

of graphene possesses at the energy of the $pp\pi$ interaction, due to the saddle point of the π and π^* bands at the M point of the first Brillouin zone (see Fig. 1).

A geometrical deformation of a nanotube affects its band structure. For instance, a uniaxial stress changes the band gap of the nanotube [35,36], simply because it modifies the bond lengths unequivalently, depending on the orientation of the bonds with respect to the axis. It has no qualitative effects on an armchair nanotube, which remains metallic because the mirror symmetry is not affected by a uniaxial strain. A twist, by contrast, opens a gap at Fermi level of the armchair tubes [37]. Bending a nanotube increases the mixing of the σ and π states and increases the DOS below the Fermi energy in the armchair nanotubes [37]. Local defects (impurity, vacancy, Stone–Wales defect, pentagon–heptagon pair, cap,...) may induce strong perturbations on the electronic structure [38], especially in armchair nanotubes. Backscattering of Bloch waves by a defect may indeed lead to oscillations of the density of states due to quantum interferences [39]. These oscillations have been detected by scanning tunneling spectroscopy [16,40].

4. Optical properties

Resonances in the Raman scattering cross section [41] and the positions of strong absorption bands in optical spectroscopy [42,43] of a nanotube are determined by electronic transitions $v_\ell \to c_{\ell'}$ between valence and conduction bands. For symmetry reasons, transitions with $\ell' \neq \ell$ have a much smaller intensity than those with $\ell' = \ell$, at least in achiral nanotubes [44]. The joint density of states (JDOS) can therefore be approximated by

$$\rho(h\nu) = 2\sum_{\kappa}\sum_{\ell}\delta\big(E_{c,\ell}(\kappa) - E_{v,\ell}(\kappa) - h\nu\big). \tag{5}$$

The bands close to the Fermi level have essentially a π character with nearly electron–hole symmetry, which means $E_{v,\ell} \approx -E_{c,\ell}$. As a result, $\rho(h\nu) \approx (1/2)n(h\nu/2)$ where n is the density of states. As a consequence, the JDOS has peaks at energies twice those of the van Hove singularities. The transition energies $\Delta E_{\ell\ell} = 2E_\ell$ increase with decreasing diameter. For small tubes, they also depend on the chirality [42]. Within the graphene zone-folding approximation and linear dispersion law (Eq. (1)), the joint density of states can be obtained analytically [27]. The expression per length unit of nanotube is

$$\rho(h\nu) \approx \rho_0 + \frac{2}{\pi\hbar v_F}\sum_{\ell} g_\ell \frac{h\nu}{\sqrt{(h\nu)^2 - \Delta E_{\ell\ell}^2}}\theta(h\nu - \Delta E_{\ell\ell}), \tag{6}$$

where θ is the Heaviside function (0 for a negative argument, 1 for a positive argument), $\rho_0 = 0$ or $2/\pi\hbar v_F$ for a semiconductor or a metal, respectively, and g_ℓ is the degeneracy of the bands, 1 or 2 for a semiconducting or a metallic nanotube, respectively. Comparison with the curves plotted in Fig. 5 shows that this last equation gives acceptable results for $h\nu < 2.5$ eV.

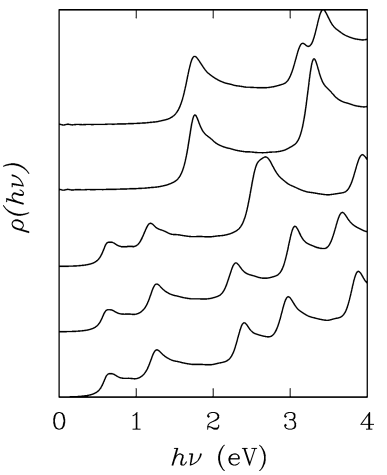

Fig. 5. Tight-binding joint density of states of five nanotubes with similar diameters. The curves were smoothed by a Lorentzian broadening of 0.07 eV FWHM. From bottom to top: $(10, 9)$, $(13, 6)$, $(17, 0)$, $(10, 10)$ and $(13, 7)$. The last two nanotubes are metallic.

Fig. 5. Densité d'états jointe de cinq nanotubes de diamètres voisins. Les courbes ont été adoucies par un élargissement lorentzien de 0.07 eV FWHM. De bas en haut : $(10, 9)$, $(13, 6)$, $(17, 0)$, $(10, 10)$ et $(13, 7)$. Les deux derniers nanotubes sont métalliques.

The joint densities of states (Eq. (5)) of five nanotubes with similar diameter around 1.4 nm are plotted in Fig. 5. For that value of the diameter, the semiconducting tubes have a pair of peaks at 0.6 (band gap) and 1.2 eV, and other resonances above 2.3 eV. The metallic tubes have a strong spike at 1.7 eV (width of the metallic plateau) and other peaks above 3 eV. On the experimental side, typical absorption spectra of nanotube ropes show two main bands centered on 0.75 and 1.3 eV, attributed to ΔE_{11} and ΔE_{22} transitions in semiconducting tubes, and a third peak at 1.9 eV due to the metallic nanotubes [42,45]. Recently, individual SWNTs isolated in cylindrical micelles were prepared in water solution. Their absorbance spectra showed a series of narrow peaks arising from specific tube diameters, corresponding to the ΔE_{11} band gap and the ΔE_{22} transition in semiconductor nanotubes [46]. As a final remark, the intensity of the Raman lines of ropes of single-wall nanotubes varies strongly when the laser excitation energy varies between 1.5 to 2.2 eV, which is due to a resonant enhancement of the metallic components when the incoming or outgoing light energy matches the ΔE_{11} transition [11].

5. Electronic properties of ropes of single-wall nanotubes and multiwall nanotubes

In ropes of SWNTs, intertube interactions, although small, are sufficient to reduce the symmetry and to modify the electron density of states of the coupled system compared to that of the isolated tubes. Early first-principle calculations for a highly-symmetric arrangement of $(6, 6)$ nanotubes on a triangular lattice indicated that this crystalline system is a zero-gap semiconductor [47]. In a close packed triangular lattice of $(10, 10)$ nanotubes, ab-initio calculations revealed the presence of a pseudo-gap of 0.1 eV width at the Fermi level [48]. Due to the reduction of symmetry, there is no crossing of π and π^* bands anymore for wave vectors parallel to the axis, but the bands disperse *versus* the component of the Bloch vector normal to the axis and they overlap each other. This is why a real gap does not form. This pseudo-gap is already present when only three nanotubes are packed on a triangle [28]. It has been detected by STS measurements on ropes of SWNTs [23]. Interestingly, a crystalline rope of $(10, 0)$ nanotubes is predicted to be metallic because the dispersion of the bands in directions normal to the axis is sufficient to close the gap of the isolated $(10, 0)$ nanotube [26].

On the experimental side, the electronic structure of multiwall nanotubes (MWNT) is less documented than for single-walled tubes. Valence-band photoemission indicates that a MWNT resembles semimetallic graphite [49]. However, both semiconducting and metallic characteristics were found by STS measurements performed on individual MWNTs [50,51]. This observation probably indicates that the STM probes only the external layer of the nanotube [52]. Furthermore, the STS spectra may vary strongly from one place to another on the same tube [53], which may be due to the presence of defects.

On the theory side, multiwall nanotubes have been the subject of several studies. Band-structure calculations have been performed exclusively for monochiral systems, most particularly zig–zag and armchair. Early tight-binding calculations performed for double-wall nanotubes (DWNT) showed that the interlayer interactions can couple some of the electron bands

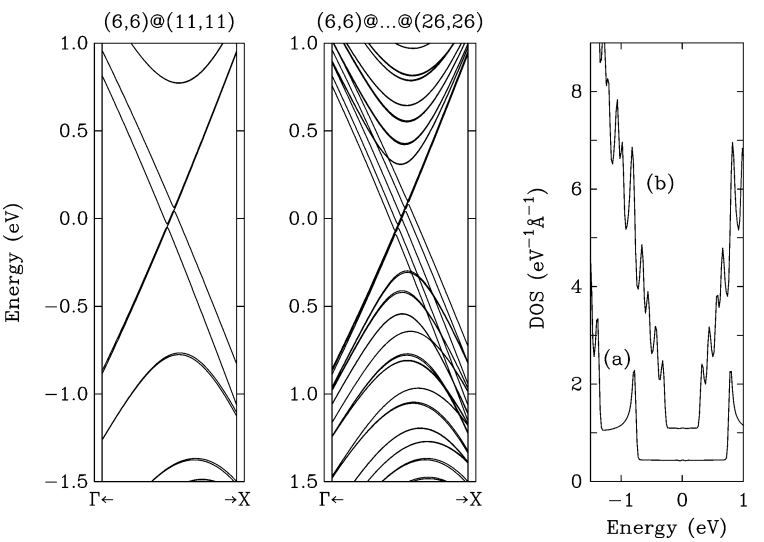

Fig. 6. Details of the band structure and density of states of (a) the two-wall $(6, 6)@(11, 11)$ nanotube and (b) the five-wall $(6, 6)@(11, 11)...@(26, 26)$ nanotube (adapted from [55]; published with permission of World Scientific).

Fig. 6. Détails de la structure de bandes et de la densité d'états électroniques du (a) nanotube bifeuillet $(6, 6)@(11, 11)$ et (b) nanotube à cinq feuillets $(6, 6)@(11, 11)...@(26, 26)$ (adapté de [55] ; publié avec la permission de World Scientific).

of the layers when they are commensurate [54], as for example in $(5,5)@(10,10)$ or $(9,0)@(18,0)$. Further calculations demonstrated that a system like $(5,5)@(10,10)$ can be a metal or a semimetal, depending on the relative position of one layer with respect to the other [55,56]. When the $(5,5)$ and $(10,10)$ coaxial layers have no mirror plane in common, the crossing between the π and π^* bands at the Fermi level becomes forbidden by group theory, and the coupled system may be driven in a semimetallic state [55]. As a result, a pseudo-gap opens near the Fermi level [56]. The argument from group theory is a fortiori valid for non-commensurate systems like $(6,6)@(11,11)$, which have no common rotational symmetry. But there, the interlayer interaction becomes so small, due to the incommensurability, that there is very little coupling between the bands of the two layers, see Fig. 6.

In general, the effects of the interlayer coupling on the density of states are small. The DOS of the two-wall and the five-wall nanotubes shown in Fig. 6 are merely the sum of the densities of states of the constituent single-wall nanotubes. This remains quite true even for commensurate MWNTs like $(5,5)@(10,10)@(15,15)$ [28]. Calculations also indicate that DWNTs mixing metallic and semiconducting layers retain the basic properties of the uncoupled constituents [54]. The intertube interactions only induce a small continuous distribution of states in the band gap of the semiconducting layer [52].

6. Applications

The fact that metallic and semiconducting nanotubes can be joined together on the same molecule [39,57] opens the way to realize pure carbon devices that can behave like a Schottky diode [58]. Such a junction often appears in the form of a kinked structure due to the presence of pentagon-heptagon pair that is needed to interconnect two nanotubes with different helicities [59], although straight junctions have also been identified [60]. In a junction between a semiconductor and a metallic nanotube, the current can flow easily in one direction and much less easily in the other direction [61,62], with the advantage that switching between these two states is very fast. And indeed rectifying current-voltage characteristics have been recorded in a kinked single-wall nanotube [63]. Here, the rectification is that of a n-type semiconductor connected to a metal [64]. Kinked multiwall nanotubes have also been observed with an asymmetric current-voltage curve, which is attributed to a junction between two semiconductors with different band gaps [65].

Since nanotubes are one-dimensional objects, dipole charges that may form at a metal-semiconductor junction do not generate a macroscopic electric field like in the case of planar junction between three-dimensional materials [62]. This geometric property has important effects in metallic contacts with a nanotube, which behave like Schottky barriers and may control the current-voltage characteristics of the system [66–68]. This means that measuring the intrinsic transport properties of a nanotube device is extremely difficult. An additional perturbation comes from the contamination of the interface between a

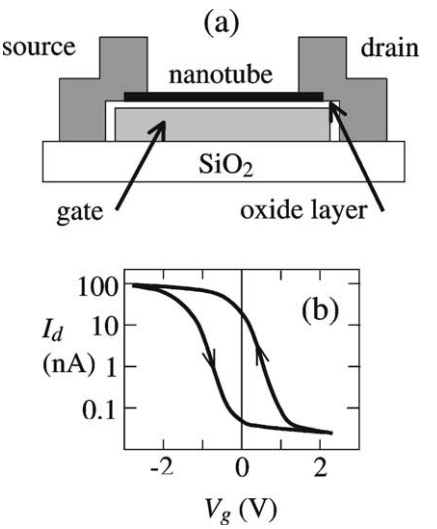

Fig. 7. (a) Schematic view of a nanotube FET device with its three metallic electrodes (adapted from [72]). (b) Hysteresis behavior of the drain current in a SWNT FET exposed to air *versus* gate voltage at a constant 10 mV bias (adapted from [76]).

Fig. 7. (a) Vue schématique d'un dispositif FET à nanotube avec ses trois électrodes métalliques (adaptée de [72]). (b) Hystérèse du courant de drain dans un FET à nanotube monofeuillet exposé à l'air en fonction de la tension de porte pour une différence de potentiel source-drain maintenue à 10 mV (adapté de [76]).

carbon nanotube and the contact electrodes by impurities and oxygen molecules, for the latter are responsible for inducing a p-type characteristic on a semiconducting nanotube [69].

The most spectacular potential application of semiconducting nanotubes in nanoelectronics [5] is their use as three-terminal devices that work like field-effect transistors (FET) [70,71]. Here, a nanotube is attached to two metallic electrode lines, acting respectively as a source and a drain. The nanotube is separated from a third electrode, the gate, by a thin insulating layer, see Fig. 7(a). Due to the difference of work function between the nanotube and the contact electrodes, Shottky barriers are formed, with a bending of the valence and conduction bands of the nanotube, and the device has a very small conductivity for a small drain–source bias. The conductivity of the nanotube can increase by several orders of magnitude by varying the gate voltage a few volts across a threshold value. This is because the gate electric field reduces the width of the Schottky barriers and, when it reaches a threshold value, the gate field injects charge carriers on the nanotube by capacitive effects [66,67]. In today devices, the insulating oxide layer between the gate and the nanotube is very thin [72,73]. Thanks to a high coupling to the nanotube, the gate signal can now be amplified to a level such that the output voltage of a first transistor can control the input of a second one. This important technological improvement, plus the fact that both p-type, n-type, and ambipolar carbon nanotube FET transistors can be realized, makes it possible to integrate the nanotubes into elementary logical gates [72,74].

Semiconducting SWNTs can also display memory effects [68]: it has been discovered that the drain current of a nanotube FET exposed to air can present an hysteresis loop when the gate voltage varies continuously between a negative value (conducting p-type semiconductor) to a positive value (non-conducting device) and back to negative values [75,76], see Fig. 7(b). It seems that charges trapped on oxidation related defects are responsible for a sizable offset of the gate voltage threshold required to switch from high to low and from low to high conductivity states. As a result, the conductance of the nanotube at low gate potential presents two stable values that may differ by a few orders of magnitude, depending on whether a large positive or negative voltage pulse was initially applied to the gate electrode. By keeping track of its gate voltage history for several days, the device works like a programmable ROM memory.

Many efforts remain to be made to transpose these prototype transistors and memories to practical device applications. The challenge is of course to control the electronic properties of the nanotubes, to manipulate and assemble thousands of them at predetermined positions on contact lines during a real device fabrication. The fact that the metallic components (approximately one third of the nanotubes) in a bundle can be burnt off by sending an appropriate pulse of current through them [77] or can be transformed into semiconductors by oxidation [76] is already a big step forward in the control process.

Acknowledgements

This work has been partly supported by the IUAP program P5/01 “Quantum size effects in nanostructured materials” of the Belgian Office for Scientific, Technical, and Cultural affairs (OSTC).

References

[1] J.W. Mintmire, B.I. Dunlap, C.T. White, Phys. Rev. Lett. 68 (1992) 631–634.
[2] N. Hamada, S.I. Sawada, A. Oshiyama, Phys. Rev. Lett. 68 (1992) 1579–1581.
[3] K. Tanaka, K. Okahara, M. Okada, T. Yamabe, Chem. Phys. Lett. 191 (1992) 469–472.
[4] R. Saito, M. Fujita, G. Dresselhaus, M.S. Dresselhaus, Appl. Phys. Lett. 60 (1992) 2204–2206.
[5] Ph. Avouris, Chem. Phys. 281 (2002) 429–445.
[6] J.L. Brédas, B. Thémans, J.M. André, R.R. Chance, R. Silbey, Synth. Metals 9 (1984) 265.
[7] R. Saito, M. Fujita, G. Dresselhaus, M.S. Dresselhaus, Phys. Rev. B 46 (1992) 1804–1811.
[8] K. Tanaka, H. Ago, T. Yamabe, K. Okahara, M. Okada, Intern. J. Quantum Chem. 63 (1997) 637–644.
[9] C.L. Kane, L. Balents, M.P.A. Fisher, Phys. Rev. Lett. 79 (1997) 5086–5089.
[10] P.R. Wallace, Phys. Rev. 71 (1947) 622–634.
[11] M.A. Pimenta, A. Marucci, S.A. Empedocles, M.G. Bawendi, E.B. Hanlon, A.M. Rao, P.C. Eklund, R.E. Smalley, G. Dresselhaus, M.S. Dresselhaus, Phys. Rev. B 58 (1998) R16016–R16019.
[12] C.T. White, D.H. Robertson, J.W. Mintmire, Phys. Rev. B 47 (1993) 5485–5488.
[13] J.W.G. Wildoer, L.C. Venema, A.G. Rinzler, R.E. Smalley, C. Dekker, Nature 391 (1998) 59–62.
[14] T.W. Odom, J.L. Huang, Ph. Kim, Ch.M. Lieber, Nature 391 (1998) 62–64.
[15] S.G. Lemay, J.W. Janssen, M. van den Hout, M. Mooij, M.J. Bronikowski, P.A. Willis, R.E. Smalley, L.P. Kouwenhoven, C. Dekker, Science 412 (2001) 617–620.
[16] M. Ouyang, J.L. Huang, C.M. Lieber, Phys. Rev. Lett. 88 (2002) 066804.
[17] C.L. Kane, E.J. Mele, Phys. Rev. Lett. 78 (1997) 1932–1935.
[18] P.E. Lammert, V.H. Crespi, Phys. Rev. B 61 (2000) 7308–7311.
[19] A. Kleiner, S. Eggert, Phys. Rev. B 64 (2001) 113402.

[20] J.W. Mintmire, C.T. White, Carbon 33 (1995) 893–902.
[21] A. Ugawa, A.G. Rinzler, D.B. Tanner, Phys. Rev. B 60 (1999) R11305–R11308.
[22] C. Zhou, J. Kong, H. Dai, Phys. Rev. Lett. 84 (2000) 5604–5607.
[23] M. Ouyang, J.L. Huang, C.L. Cheung, C.M. Lieber, Science 292 (2001) 702–705.
[24] J.Y. Yi, J. Bernholc, Phys. Rev. B 47 (1993) 1708–1711.
[25] X. Blase, L.X. Benedict, E.L. Shirley, S.G. Louie, Phys. Rev. Lett. 72 (1994) 1878–1881.
[26] S. Reich, C. Thomsen, P. Ordejón, Phys. Rev. B 65 (2002) 155411.
[27] J.W. Mintmire, C.T. White, Phys. Rev. Lett. 81 (1998) 2506–2509.
[28] A. Rubio, Appl. Phys. A 68 (1999) 275–282.
[29] S. Reich, J. Maultzsch, C. Thomsen, P. Ordejón, Phys. Rev. B 66 (2002) 035412.
[30] Ph. Lambin, A.A. Lucas, Phys. Rev. B 56 (1997) 3571–3573.
[31] P.J. Lin-Chung, A.K. Rajagopal, J. Phys.: Condens. Matter 6 (1994) 3697–3706.
[32] Ph. Kim, T. Odom, J.L. Huang, C.M. Lieber, Phys. Rev. Lett. 82 (1999) 1225–1228.
[33] J.C. Charlier, Ph. Lambin, Phys. Rev. B 57 (1998) R15037–R15039.
[34] R. Saito, G. Dresselhaus, M.S. Dresselhaus, Phys. Rev. B 61 (2000) 2981–2990.
[35] R. Heyd, A. Charlier, E. McRae, Phys. Rev. B 55 (1997) 6820–6823.
[36] L. Yang, M.P. Anantram, J. Han, J.P. Lu, Phys. Rev. B 60 (1999) 13874–13878.
[37] A. Rochefort, Ph. Avouris, F. Lesage, D.R. Salahub, Phys. Rev. B 60 (1999) 13824–13830.
[38] J.C. Charlier, Accounts Chem. Res. 35 (2002) 1063–1069.
[39] Ph. Lambin, A. Fonseca, J.P. Vigneron, J.B. Nagy, A.A. Lucas, Chem. Phys. Lett. 245 (1995) 85–89.
[40] L.C. Venema, J.W.G. Wildoer, J.W. Janssen, S.J. Tans, H.L.J. Temminck Tuinstra, L.P. Kouwenhoven, C. Dekker, Science 283 (1999) 52–55.
[41] A.M. Rao, E. Richter, S. Bandow, B. Chase, P.C. Eklund, K.A. Williams, S. Fang, K.R. Subbaswamy, M. Menon, A. Thess, R.E. Smalley, G. Dresselhaus, M.S. Dresselhaus, Science 275 (1997) 187–191.
[42] H. Kataura, Y. Kumazawa, Y. Maniwa, I. Umezu, S. Suzuki, Y. Ohtsukada, Y. Achiba, Synt. Metals 103 (1999) 2555–2558.
[43] P. Petit, C. Mathis, C. Journet, P. Bernier, Chem. Phys. Lett. 305 (1999) 370–374.
[44] E. Richter, K.R. Subbaswamy, Phys. Rev. Lett. 79 (1997) 2738–2741.
[45] O. Jost, A.A. Gorbunov, W. Pompe, T. Pichler, R. Friedlein, M. Knupfer, M. Reibold, H.D. Bauer, L. Dunsch, M.S. Golden, J. Fink, Appl. Phys. Lett. 75 (1999) 2217–2219.
[46] M.J. OConnell, S.M. Bachilo, C.B. Huffman, V.C. Moore, M.S. Strano, E.H. Haroz, K.L. Rialon, P.J. Boul, W.H. Noon, C. Kittrell, J. Ma, R.H. Hauge, R.B. Weisman, R.E. Smalley, Science 297 (2002) 593–596.
[47] J.C. Charlier, X. Gonze, J.P. Michenaud, Europhys. Lett. 29 (1995) 43–48.
[48] P. Delaney, H.J. Choi, J. Ihm, S.G. Louie, M.L. Cohen, Nature 391 (1998) 466–468.
[49] P. Chen, X. Wu, X. Sun, J. Lin, W. Ji, K.L. Tan, Phys. Rev. Lett. 82 (1999) 2548–2551.
[50] C.H. Olk, J.P. Heremans, J. Mater. Res. 9 (1994) 259–262.
[51] A. Hassanien, M. Tokumoto, S. Ohshima, Y. Kuriki, F. Ikazaki, K. Uchida, M. Yumara, Appl. Phys. Lett. 75 (1999) 2755–2757.
[52] Ph. Lambin, V. Meunier, A. Rubio, Phys. Rev. B 62 (2000) 5129–5135.
[53] L.P. Biró, P.A. Thiry, Ph. Lambin, C. Journet, P. Bernier, A.A. Lucas, Appl. Phys. Lett. 73 (1998) 3680–3682.
[54] R. Saito, G. Dresselhaus, M.S. Dresselhaus, J. Appl. Phys. 73 (1993) 494–500.
[55] Ph. Lambin, J.C. Charlier, J.P. Michenaud, in: H. Kuzmany, J. Fink, M. Mehring, S. Roth (Eds.), Progress in Fullerene Research, World Scientific, Singapore, 1994, pp. 130–134.
[56] Y.K. Kwon, D. Tomanek, Phys. Rev. B 58 (1998) R16001–R16004.
[57] L. Chico, V.H. Crespi, L.X. Benedict, S.G. Louie, M.L. Cohen, Phys. Rev. Lett. 76 (1996) 971–974.
[58] R.F. Service, Science 271 (1996) 1232.
[59] B.I. Dunlap, Phys. Rev. B 49 (1994) 5643–5649.
[60] M. Ouyang, J.L. Huang, Ch.M. Lieber, Science 291 (2001) 97–100.
[61] A.O. Odintsov, Phys. Rev. Lett. 85 (2000) 150–153.
[62] F. Leonnard, J. Tersoff, Phys. Rev. Lett. 84 (2000) 4693–4696.
[63] Z. Yao, H.W.Ch. Postma, L. Balents, C. Dekker, Nature 402 (1999) 273–276.
[64] T. Yamada, Appl. Phys. Lett. 80 (2002) 4027–4029.
[65] J.O. Lee, H. Oh, J.R. Kim, K. Kang, J.J. Kim, J. Kim, K.H. Yoo, Appl. Phys. Lett. 79 (2001) 1351–1353.
[66] S. Heinze, J. Tersoff, R. Martel, V. Derycke, J. Appenzeller, Ph. Avouris, Phys. Rev. Lett. 89 (2002) 106801.
[67] J. Appenzeller, J. Knoch, V. Derycke, R. Martel, S. Wind, Ph. Avouris, Phys. Rev. Lett. 89 (2002) 126801.
[68] M. Radosavljevic, M. Freitag, K.V. Thadani, A.T. Johnson, Nano Lett. 2 (2002) 761–764.
[69] P.G. Collins, K. Bradley, M. Ishigami, A. Zettl, Science 287 (2000) 1801–1804.
[70] S.T. Tans, A.R.M. Verschueren, C. Dekker, Nature 393 (1998) 49–52.
[71] R. Martel, T. Schmidt, H.R. Shea, T. Hertel, Ph. Avouris, Appl. Phys. Lett. 73 (1998) 2447–2449.
[72] A. Bachtold, P. Hadley, T. Nakanishi, C. Dekker, Science 294 (2001) 1317–1320.
[73] S. Wind, J. Appenzeller, R. Martel, V. Derycke, Ph. Avouris, Appl. Phys. Lett. 80 (2002) 3817–3819.
[74] V. Derycke, R. Martel, J. Appenzeller, Ph. Avouris, Nano Lett. 1 (2001) 453–456.
[75] M.S. Fuhrer, B.M. Kim, T. Dürkop, T. Brintlinger, Nano Lett. 2 (2002) 755–759.
[76] J.B. Cui, R. Sordan, M. Burghard, K. Kern, Appl. Phys. Lett. 81 (2002) 3260–3262.
[77] P.G. Collins, M.S. Arnold, Ph. Avouris, Science 292 (2001) 706–709.